biosensors

MDPI

Article

Detection of Hypoxanthine from Inosine and Unusual Hydrolysis of Immunosuppressive Drug Azathioprine through the Formation of a Diruthenium(III) System

Marta Orts-Arroyo, Isabel Castro and José Martínez-Lillo *

Instituto de Ciencia Molecular (ICMol), Universitat de València, c/ Catedrático José Beltrán 2, Paterna, 46980 València, Spain; marta.orts-arroyo@uv.es (M.O.-A.); isabel.castro@uv.es (I.C.)
* Correspondence: f.jose.martinez@uv.es; Tel.: +34-9635-44460

Abstract: Hypoxanthine (hpx) is an important molecule for both biochemistry research and biomedical applications. It is involved in several biological processes associated to energy and purine metabolism and has been proposed as a biomarker for a variety of disease states. Consequently, the discovery and development of systems suitable for the detection of hypoxanthine is pretty appealing in this research field. Thus, we have obtained a stable diruthenium (III) compound in its dehydrated and hydrated forms with formula $[\{Ru(\mu\text{-}Cl)(\mu\text{-}hpx)\}_2Cl_4]$ (**1a**) and $[\{Ru(\mu\text{-}Cl)(\mu\text{-}hpx)\}_2Cl_4]\cdot 2H_2O$ (**1b**), respectively. This purine-based diruthenium(III) system was prepared from two very different starting materials, namely, inosine and azathioprine, the latter being an immunosuppressive drug. Remarkably, it was observed that an unusual azathioprine hydrolysis occurs in the presence of ruthenium, thus generating hypoxanthine instead of the expected 6-mercaptopurine antimetabolite, so that the hpx molecule is linked to two ruthenium(III) ions. **1a** and **1b** were characterized through IR, SEM, powder and single-crystal X-ray Diffraction and Cyclic Voltammetry (CV). The electrochemical studies allowed us to detect the hpx molecule when coordinated to ruthenium in the reported compound. The grade of sensitivity, repeatability and stability reached by this diruthenium system make it potentially useful and could provide a first step to develop new sensor devices suitable to detect hypoxanthine.

Keywords: hypoxanthine; inosine; azathioprine; 6-mercaptopurine; biomarker; ruthenium

Citation: Orts-Arroyo, M.; Castro, I.; Martínez-Lillo, J. Detection of Hypoxanthine from Inosine and Unusual Hydrolysis of Immunosuppressive Drug Azathioprine through the Formation of a Diruthenium(III) System. *Biosensors* **2021**, *11*, 19. https://doi.org/10.3390/bios11010019

Received: 24 November 2020
Accepted: 6 January 2021
Published: 11 January 2021

1. Introduction

Hypoxanthine (6-hydroxypurine) is a deaminated form of adenine and a constituent of the nucleoside inosine (Scheme 1). It is formed during purine metabolism and is found in both tissues and body fluids of human beings and animals. The identification of hypoxanthine (hpx) as a biomarker for hypoxia has long been known [1,2]. More recently, hpx has also been proposed as a biomarker for colorectal cancer [3], Alzheimer's disease [4], multiple sclerosis [5] and cardiac ischemia [6] and as checkpoint metabolite for other inflammatory processes [7] and toxicity levels [8]. In addition, hpx has been studied as a strong predictor of performance in highly trained athletes in sports and physical exertion, the hpx concentration indicating the training status and adaptation in consecutive phases of long training cycles [9,10]. Moreover, the determination of levels of hpx in meat and fish products has been established to be an important and convenient indicator of freshness and quality control in the food industry [11,12].

As a continuation of our interest in investigating biomolecule-based complexes of several metal ions [13–17] and their implementation in devices [18,19], we have studied the synthesis of ruthenium with some purine-based compounds that either contain hypoxanthine or could generate this analyte. Thus, we have investigated the products of the hydrolysis reactions with inosine and azathioprine (Scheme 1).

The nucleoside inosine is formed by a hpx molecule that is connected to a ribose ring through N(9)-glycosidic bond. It belongs to a group of purine antimetabolites recommended for treatment of measles and herpes infections, among others [20]. Studies on the inosine hydrolysis have been previously reported [21,22]. Azathioprine is a slow-release prodrug of the antimetabolite 6-mercaptopurine (Scheme 1), which is used as an anticancer and immunosuppressive drug [23,24]. It is used as an established clinical agent for the treatment of several pathologies, such as rheumatoid arthritis, ulcerative colitis, systemic lupus and Crohn's disease, and also as an anti-rejection medication in human organ transplantation [23,24]. The N-methylnitroimidazolyl group of the azathioprine molecule protects the active form 6-mercaptopurine. Azathioprine undergoes hydrolysis in vivo to alter the metabolism and distribution of the drug toward its target [23,24].

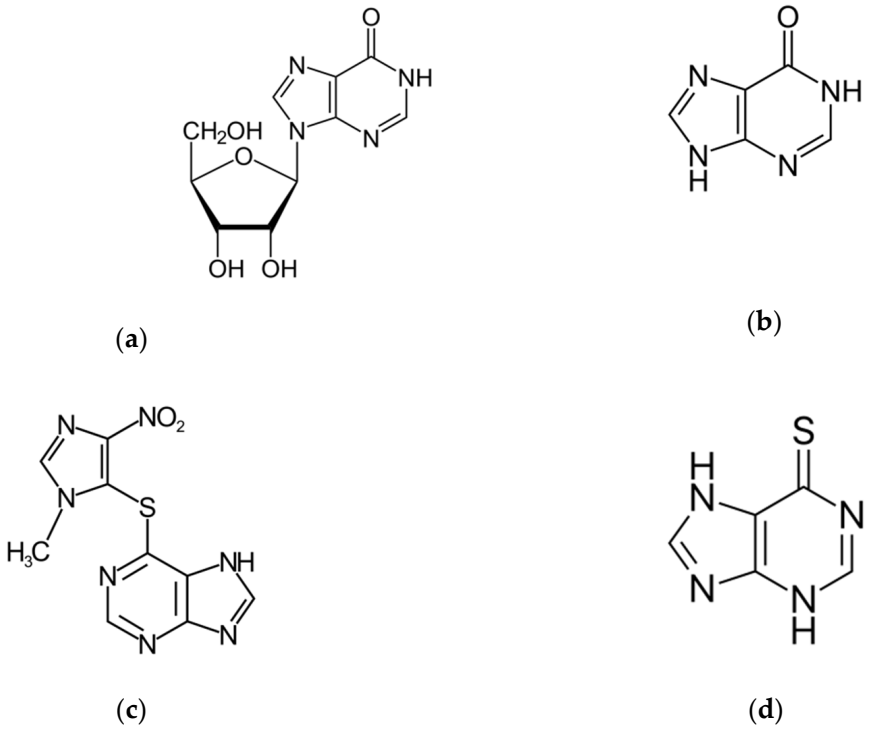

Scheme 1. Molecular structure of: (**a**) Inosine, (**b**) Hypoxanthine, (**c**) Azathioprine and (**d**) 6-Mercaptopurine.

Previously reported methods of determination of hpx include high-performance liquid chromatography [25–28], capillary electrophoresis [29,30], spectrophotometry [31,32] and electrochemiluminescence [33,34], which are usually costly and laborious and require a long analysis time. On the other hand, electrochemical methods offer several advantages, such as relatively simple and cheap instrumentation, high selectivity and sensitivity, high stability and rapid response time [35–37]. Nevertheless, given the wide range of potentially interfering purine-based compounds that can affect the detection of hpx generated in biological processes, more selective methods of analysis are needed.

Herein, we report the preparation, characterization and electrochemical properties of a new diruthenium system (Figure 1), which shows great stability and also selectivity for the hypoxanthine molecule, and therefore, could establish a first step to develop new sensor devices suitable for hypoxanthine detection.

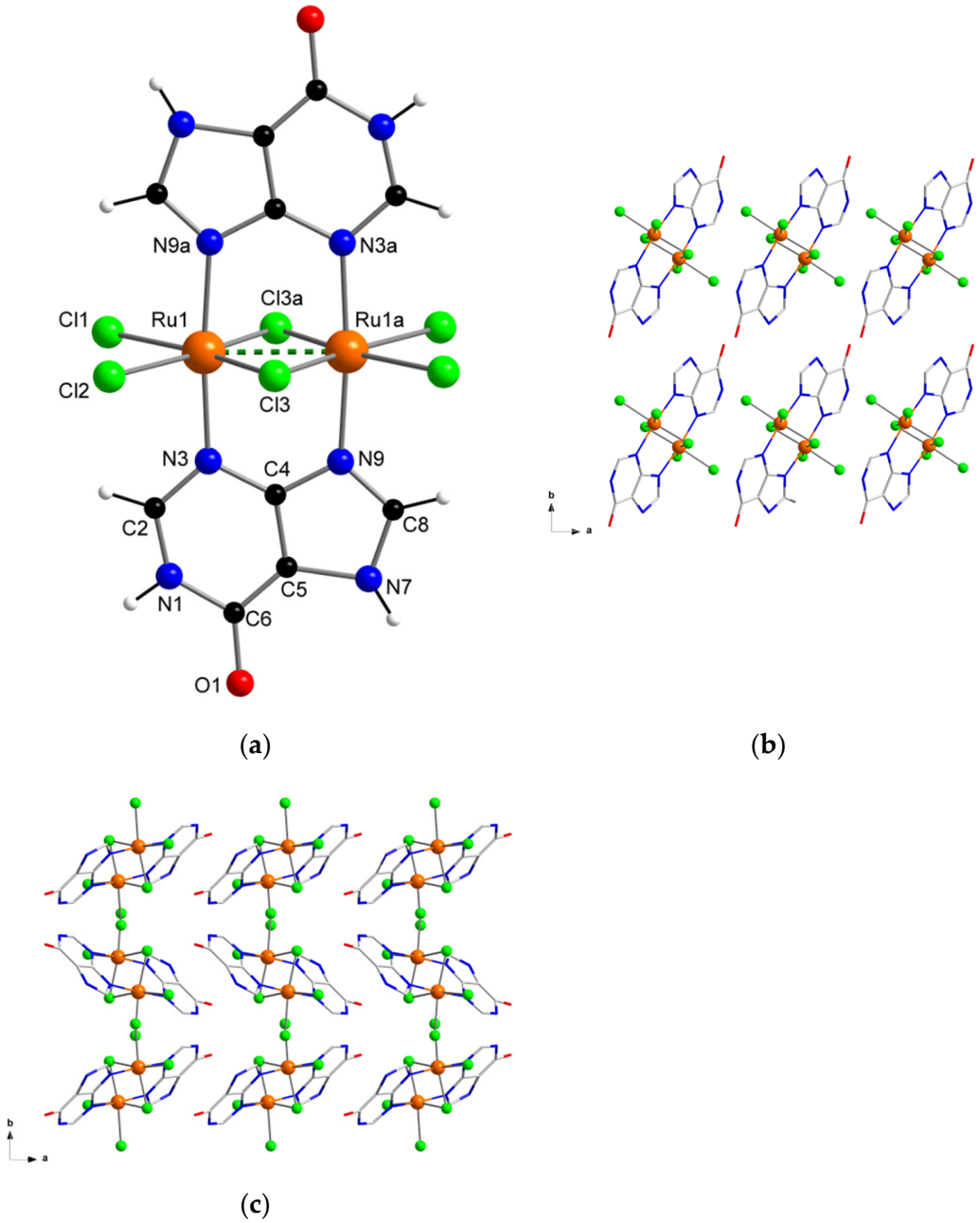

Figure 1. (**a**) Molecular structure of the [{Ru(μ-Cl)(μ-hpx)}$_2$Cl$_4$] complex in **1a** and **1b**; (**b**) view along the crystallographic *c* axis of a fragment of the crystal packing of **1a**; (**c**) view along the crystallographic *c* axis of a fragment of the crystal packing of **1b**.

2. Materials and Methods

2.1. Reagents and Instruments

All of the manipulations were performed under aerobic conditions. Azathioprine and inosine were purchased from Alfa Aesar and Sigma Aldrich, respectively. Ruthenium precursors, $RuCl_3 \cdot H_2O$ and $K_2[RuCl_5(H_2O)]$, and the rest of materials were used as-received and were of reagent grade. Elemental analyses (C, H, N) and X-ray microanalysis were performed by the Central Service for the Support to Experimental Research (SCSIE) at the University of Valencia. Scanning electron microscopy (SEM) images and results were obtained from a Hitachi S-4800 field emission scanning electron microscope. Infrared spec-

tra (IR) of **1a** and **1b** (in the Supplementary Materials) were recorded with a PerkinElmer Spectrum 65 FT-IR spectrometer in the range of 400 to 4000 cm^{-1} (Figure 2).

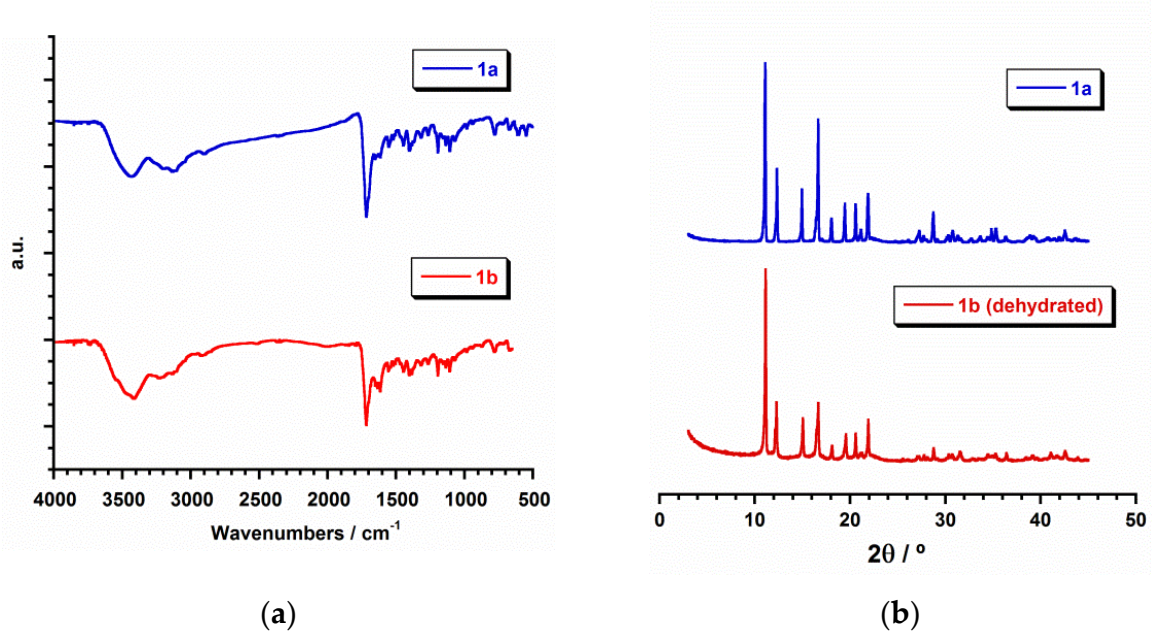

Figure 2. (**a**) IR spectra (Transmission mode) for **1a** (blue) and **1b** (red); (**b**) plot of the experimental powder X-ray diffraction (PXRD) patterns profile (2θ/°) in the range 0–50° for **1a** (blue) and dehydrated **1b** (red).

Electrochemical studies were performed by using an Autolab/PGSTAT 204 scanning potentiostat operating at a scan rate range of 10–250 mV s^{-1}. Cyclic voltammograms were carried out by using 0.1 M NBu_4PF_6 as supporting electrolyte and 0.001 M solutions of **1a**, inosine and azathioprine in dry dimethylformamide (dmf). The working electrode was a glassy carbon disk (0.32 cm^2) that was polished with 1.0 μm of diamond powder, sonicated, washed with absolute ethanol and acetone and air dried. The reference electrode was AgCl/Ag, separated from the test solution by a salt bridge containing the solvent/supporting electrolyte, with platinum as an auxiliary electrode. All experiments were performed in standard electrochemical cells at 25 °C under argon. The investigated potential range was in the range of −2.0 to +2.0 V vs. AgCl/Ag. Ferrocene (F_c) was added as internal standard at the end of all the measurements. The formal potentials were measured at a scan rate of 200 mV s^{-1} and were referred to the ferrocenium/ferrocene (F_c^+/F_c) redox couple.

2.2. Preparation of the Compounds

2.2.1. Synthesis of $[\{Ru(\mu\text{-}Cl)(\mu\text{-}hpx)\}_2Cl_4]$ (**1a**)

A solvothermal reaction of $K_2[RuCl_5(H_2O)]$ (3.52 mg, 0.01 mmol) and inosine (2.66 mg, 0.01 mmol) was performed in HCl (4 mL, 3 M) at 90 °C for 3 days, followed by a 12-h cooling process to room temperature. Dark brown crystals of **1a** were obtained and were suitable for X-ray data collection. Yield: *ca*. 55%. Anal. Calcd. for $C_{10}H_8Cl_6N_8O_2Ru_2$ (**1a**): C, 17.5; H, 1.2; N, 16.3. Found: C, 17.7; H, 1.3; N, 16.5. IR peaks (KBr pellets, ν/cm^{-1}): 3202(m), 3132(m), 3110(m), 3046(m), 2905(m), 1718(vs), 1653(m), 1555(m), 1522(w), 1447(m), 1407(m), 1318(m), 1267(m), 1196(s), 1160(w), 1137(m), 1118(s), 984(w), 779(m), 723(w), 674(m), 610(m), 550(m), 478(w) and 412(w).

2.2.2. Synthesis of $[\{Ru(\mu\text{-}Cl)(\mu\text{-}hpx)\}_2Cl_4]\cdot 2H_2O$ (**1b**)

$RuCl_3\cdot H_2O$ (6.60 mg, 0.03 mmol) and azathioprine (6.80 mg, 0.03 mmol) reacted through a solvothermal reaction in HCl (4 mL, 3 M) at 90 °C for 3 days, followed by a 12-h cooling process to room temperature. Dark brown crystals of **1b** were thus obtained, which

were suitable for X-ray data collection. Yield: *ca.* 72%. Anal. Calcd. for $C_{10}H_{12}Cl_6N_8O_4Ru_2$ (**1b**): C, 16.6; H, 1.7; N, 15.5. Found: C, 16.7; H, 1.9; N, 15.2. IR peaks (KBr pellets, ν/cm^{-1}): 3433(br), 3202(m), 3133(m), 3110(m), 3047(m), 2905(m), 1718(vs), 1653(m), 1615(m), 1554(m), 1522(w), 1447(m), 1407(m), 1318(m), 1267(m), 1196(s), 1160(w), 1137(m), 1118(s), 984(w), 779(m), 723(w), 674(m), 610(m), 550(m), 478(w) and 412(w).

2.3. X-ray Data Collection and Structure Refinement

X-ray diffraction data from single crystals of dimensions 0.18 × 0.06 × 0.04 (**1a**) and 0.27 × 0.14 × 0.11 mm^3 (**1b**) were collected on a Bruker D8 Venture diffractometer with graphite-monochromated Mo-K_α radiation (λ = 0.71073 Å). Crystal parameters and refinement results for **1a** and **1b** are summarized in Table 1. The structures were solved by standard direct methods and subsequently completed by Fourier recycling by using the SHELXTL software packages. The obtained models were refined with version 2017/1 of SHELXL against F^2 on all data by full-matrix least squares [38]. In the two samples, all non-hydrogen atoms were anisotropically refined, whereas the hydrogen atoms of the hpx molecules were set in calculated positions and refined isotropically by using the riding model. The graphical manipulations were performed with the DIAMOND program [39]. The CCDC codes for **1a** and **1b** are 2046049 and 2046050, respectively. In addition, X-ray powder diffraction (PXRD) measurements were performed through a capillary sample holder in a PANalytical Empyrean diffractometer containing a hybrid monochromator (Cu-$K_{\alpha1}$ radiation) and a PIXcel detector.

Table 1. Summary of the crystal data and structure refinement parameters for **1a** and **1b**.

Compound	1a	1b
CCDC	2046049	2046050
Formula	$C_{10}H_8Cl_6N_8O_2Ru_2$	$C_{10}H_{12}Cl_6N_8O_4Ru_2$
M_r/g mol^{-1}	687.08	723.12
Crystal system	monoclinic	monoclinic
Space group	$P2_1/c$	$P2_1/c$
a/Å	7.161(1)	8.714(1)
b/Å	10.720(1)	11.865(1)
c/Å	11.666(1)	10.286(1)
α/°	90	90
β/°	90.81(1)	112.32(1)
γ/°	90	90
V/Å^3	895.52(9)	983.81(3)
Z	2	2
D_c/g cm^{-3}	2.548	2.441
μ(Mo-K_α)/mm^{-1}	2.611	2.390
F(000)	660.0	700.0
Goodness-of-fit on F^2	1.170	1.066
R_1 [$I > 2\sigma(I)$]	0.0726	0.0844
wR_2 [$I > 2\sigma(I)$]	0.1811	0.2014

3. Results and Discussion

3.1. Synthetic Procedure

By reacting $K_2[RuCl_5(H_2O)]$ with inosine (for **1a**) and $RuCl_3{\cdot}H_2O$ with azathioprine (for **1b**) in hydrochloric acid (3 M) solutions, we obtained the same diruthenium(III) complex, but in its dehydrated and hydrated forms [{Ru(μ-Cl)(μ-hpx)}$_2$Cl$_4$] (**1a**) and [{Ru(μ-Cl)(μ-hpx)}$_2$Cl$_4$]·2H$_2$O (**1b**), respectively. In both cases, the synthesis process was performed by heating the reaction mixture at 90 °C through a solvothermal method, followed by a 12-h cooling process to room temperature as the crystallization technique. Thus, dark brown crystals of **1a** and **1b** were obtained in satisfactory yields. Inosine was chosen in this work as starting material because it is a suitable source of hypoxanthine (Scheme 1), and given the synthetic conditions, this purine nucleoside can easily undergo hydrolysis

through a N(9)-glycosidic bond with a rapid release of hypoxanthine along with the ribose sugar [21]. The released hypoxanthine molecule acts as a ligand towards the ruthenium metal ions, generating the stable complex **1a**. In the case of the synthesis with azathioprine, **1b** was obtained as an unexpected product in a reaction which was intended to replace some of the Cl groups linked to the ruthenium(III) ions by the potentially chelating 6-mercaptopurine antimetabolite (Scheme 1). Instead, the species **1b** was formed. The hydrolytic reaction that azathioprine undergoes during its mechanism of drug action, that is, the cleavage of the N-methylnitroimidazolyl group from the sulfur atom, and therefore, the release of 6-mercaptopurine [23,24], in the presence of ruthenium(III) ions and in an acid medium, would be modified. After releasing the 6-mercaptopurine molecule, water attacks it, generating hypoxanthine, which in turn would lead to the formation of the species **1b**, so that the reported syntheses constitute new preparative methods to obtain purine-based Ru(III) compounds.

3.2. Description of the Crystal Structure

The crystal structure and exact chemical composition of **1a** and **1b** were established by single-crystal X-ray diffraction. **1a** and **1b** crystallize in the monoclinic system with space group $P2_1/c$ (Table 1). Their structures are made up of the neutral dinuclear [{Ru(μ-Cl)(μ-hpx)}$_2$Cl$_4$] units. Only in **1b** there are solvent molecules of crystallization, which are H_2O molecules. In their asymmetric units, half a [{Ru(μ-Cl)(μ-hpx)}$_2$Cl$_4$] complex is in both **1a** and **1b**, and one H_2O molecule of crystallization is also present in **1b** (Figure 1).

In the dinuclear complex of **1a** and **1b**, each six-coordinate Ru^{III} ion is bonded to four chloride ions and two nitrogen atoms (N3 and N9) from two hpx molecules in a distorted octahedral environment. No significant differences are found in the Ru–Cl [average value, 2.329(1) Å in **1a** and 2.310(1) Å in **1b**] and Ru–N [2.066(1) Å in **1a** and 2.061(1) Å in **1b**] bond lengths, which are similar in both compounds and are in agreement with those values found in previously reported Ru^{III} systems [40,41]. The two Ru^{III} ions are linked each other through two hpx molecules and a double Ru–Cl–Ru bridge and the short intramolecular Ru···Ru distance that is generated (ca. 2.6 Å) indicates the formation of a metal-metal bond (dashed line in Figure 1a). The hpx molecule in **1a** and **1b** is planar and its bond lengths and angles agree with those found in the literature for similar dinuclear complexes [42,43].

In the crystal lattice of **1a** and **1b** the dinuclear [{Ru(μ-Cl)(μ-hpx)}$_2$Cl$_4$] units pack in different ways (Figure 1b,c), because of their pseudopolymorphism. Thus, π···π stacking interactions between neighboring rings of coordinated hpx molecules occur in **1b** [with the shortest intercentroid distance being *ca*. 3.85 Å], whereas no π· · · π type interactions are observed in **1a**. Cl···π interactions between adjacent [{Ru(μ-Cl)(μ-hpx)}$_2$Cl$_4$] units take place in both Ru^{III} compounds [Cl···π distances varying in the ranges 3.16–3.37 and 3.46–3.73 Å for **1a** and **1b**, respectively]. In addition, H-bonding interactions contribute to stabilizing the crystal structure in both systems. Finally, the powder X-ray diffraction (PXRD) patterns of **1a** and **1b**, which are quite different to that of the hpx molecule [44], confirmed the homogeneity of their bulk samples (Figure 2).

3.3. Scanning Electron Microscopy (SEM)

The study of X-ray microanalysis through of scanning electron microscopy (SEM) gave an Ru/Cl molar ratio of 1:3 for both studied samples (**1a** and **1b**) and was performed as previously done for other ruthenium systems [45,46]. Sulfur was not detected in **1a** nor **1b**. The pseudopolymorphism of **1a** and **1b** was evident in the recorded images that are given in Figure 3, where crystals of **1a** are shown as needles, whereas crystals of **1b** are displayed as crystallized plates.

3.4. Cyclic Voltammetry (CV)

The electrochemical properties of the diruthenium(III) complex were investigated through cyclic voltammetry (CV) in dry dmf and at room temperature. Figure 4 shows a comparison of CV curves obtained in the same conditions for **1a**, inosine and azathio-

prine. The electrochemical behavior of azathioprine has been studied in detail in previous works [47–50]; nevertheless, we have included it for the purpose of our investigation. The most characteristic feature observed during the electrochemical reduction of azathioprine is the peak detected at a potential of about −1.30 V, which can be assigned to the reduction of the nitro group (-NO_2) to the corresponding hydroxylamine (-NHOH) that the N-methylnitroimidazolyl moiety of the molecule contains [47–50]. The CV curve obtained for inosine is very similar to that of hypoxantine, which makes the detection of hypoxantine in the presence of inosine quite difficult [51,52].

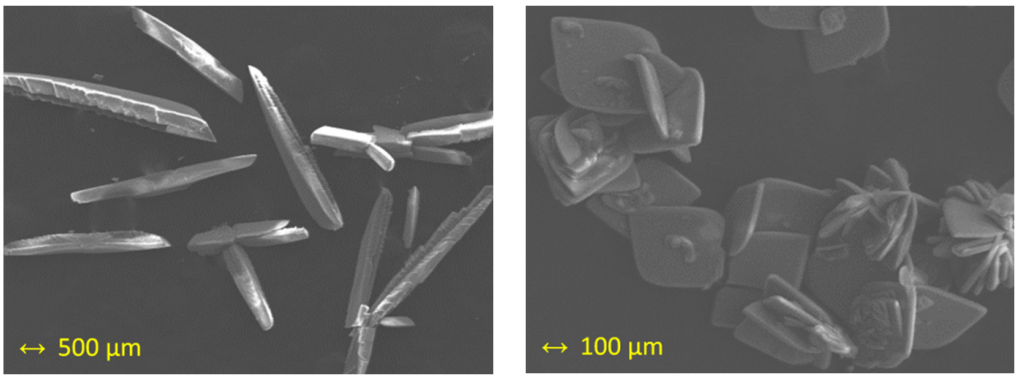

Figure 3. Scanning electron microscopy (SEM) images of: (**a**) crystals of **1a**; (**b**) crystals of **1b**.

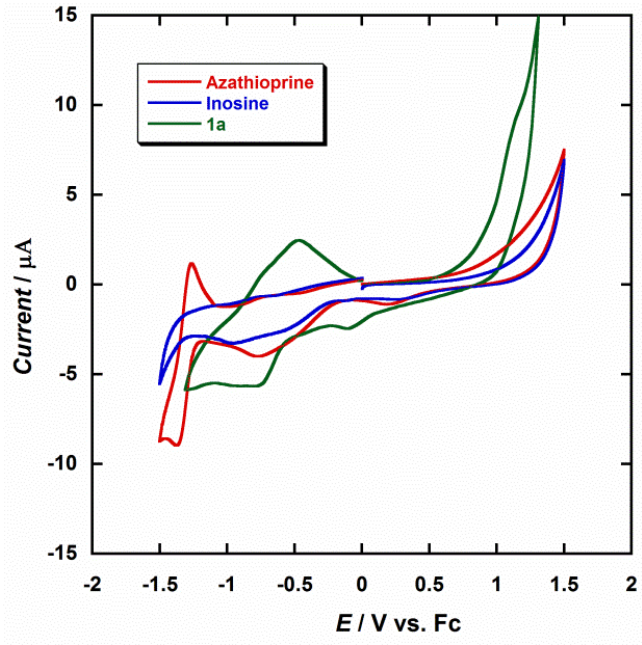

Figure 4. Cyclic voltammograms of **1a** (green), inosine (blue) and azathioprine (red) in dry dmf (0.1 M NBu_4PF_6) at 25 °C and scan rate 200 mV/s.

Diruthenium complexes exhibiting metal–metal bonding have been extensively investigated for decades [53]. In general, this type of Ru_2 compounds show electronic structures and redox properties that are unique [54–56]. Only one or up to three redox processes can be observed in the CV curves of these systems, depending on the solvent and the supporting electrolyte [54–56]. In dimethylformamide (dmf), only a single reduction would be expected, which would occur between 0.0 V and −0.30 V, so that the first reduction peak observed at −0.11 V for **1a** would be associated to the Ru^{III}/Ru^{II} reduction process, which is very close to that reported for similar Ru_2^{III} systems [54]. A second peak at −0.82 V

would be generated by the influence of the analyte, in this case the hpx molecule (Figure 4). For testing repeatability of the CV curve of the studied Ru_2^{III} system (**1a**), it was measured five times. Thus, a relative standard deviation of approximately 1.5% of the current response was obtained. It is evident from Figure 4 that there is a marked difference between the reported reductions waves for these three compounds, their current peaks being found to be well-resolved at the employed conditions, and the coordination of the hpx molecule being responsible of the CV curve observed for **1a**. Therefore, given the possibility of coexistence of hypoxanthine and inosine, or azathioprine, in singular biological processes or biomedical studies, our results can be used for the designing and development of new ruthenium-based devices that act as sensors for the detection of hypoxanthine.

4. Conclusions

In summary, a new purine-based diruthenium(III) system of formula [{Ru(μ-Cl)(μ-hpx)}$_2$Cl$_4$] (hpx = hypoxanthine) has been prepared from two different starting materials, namely, inosine and azathioprine, the latter being an immunosuppressant drug. Remarkably, it was observed that during the synthetic process azathioprine undergoes hydrolytic reaction that in the presence of ruthenium generates hpx, instead of the expected 6-mercaptopurine antimetabolite, which in turn was detected through the formation of the diruthenium(III) system. The diruthenium(III) system was obtained in its dehydrated and hydrated forms and characterized by IR, SEM, powder and single-crystal X-ray diffraction and cyclic voltammetry (CV). The study on the CV curves allowed us to detect hpx when coordinated to ruthenium in the reported compound. The grade of sensitivity, repeatability and stability reached by this diruthenium system make it potentially useful and could provide a first step to develop sensor devices suitable to detect the hpx molecule. Further investigations on the synthesis and characterization of this type of ruthenium systems is now in progress for similar target molecules in our group.

Supplementary Materials: X-ray crystallographic data in CIF format for compounds **1a** and **1b** are available online at https://www.mdpi.com/2079-6374/11/1/19/s1.

Author Contributions: I.C. and J.M.-L. conceived the idea and obtained funding for the project. M.O.-A. performed the synthesis, the X-ray data collection and the rest of the physical measurements. J.M.-L. analyzed the data associated with all the experiments and wrote the manuscript, which all authors discussed and commented on. All authors have read and agreed to the published version of the manuscript.

Funding: This research was funded by the VLC-BIOCLINIC Program (2017) of the University of Valencia [Subprogram A "*Acciones Exploratorias*", Project 02-2017-A] and the Spanish Ministry of Science, Innovation and Universities [Project PID2019-109735GB-I00].

Institutional Review Board Statement: Not applicable.

Informed Consent Statement: Not applicable.

Data Availability Statement: Not applicable.

Acknowledgments: The authors M.O.-A. and J.M.-L. thank the Spanish "FPI fellowships" and "Ramón y Cajal" programs, respectively.

Conflicts of Interest: The authors declare no conflict of interest.

References

1. Saugstad, O.D. Hypoxanthine as a Measurement of Hypoxia. *Pediatr. Res.* **1975**, *9*, 158–161. [CrossRef] [PubMed]
2. Nagao, H.; Nishizawa, H.; Tanaka, Y.; Fukata, T.; Mizushima, T.; Furuno, M.; Bamba, T.; Tsushima, Y.; Fujishima, Y.; Kita, S.; et al. Hypoxanthine Secretion from Human Adipose Tissue and its Increase in Hypoxia. *Obesity* **2018**, *26*, 1168–1178. [CrossRef] [PubMed]
3. Long, Y.; Sánchez-Espiridion, B.; Lin, M.; White, L.; Mishra, L.; Raju, G.S.; Kopetz, S.; Eng, C.; Hildebrandt, M.A.T.; Chang, D.W.; et al. Global and targeted serum metabolic profiling of colorectal cancer progression. *Cancer* **2017**, *123*, 4066–4074. [CrossRef] [PubMed]
4. Chouraki, V.; Preis, S.R.; Yang, Q.; Beiser, A.; Li, S.; Larson, M.G.; Weinstein, G.; Wang, T.J.; Gerszten, R.E.; Vasan, R.S.; et al. Association of amine biomarkers with incident dementia and Alzheimer's disease in the Framingham Study. *Alzheimer's Dement.* **2017**, *13*, 1327–1336. [CrossRef] [PubMed]

5. Lazzarino, G.; Amorini, A.M.; Petzold, A.; Gasperini, C.; Ruggieri, S.; Quartuccio, M.E.; Lazzarino, G.; Di Stasio, E.; Tavazzi, B. Serum Compounds of Energy Metabolism Impairment Are Related to Disability, Disease Course and Neuroimaging in Multiple Sclerosis. *Mol. Neurobiol.* **2017**, *54*, 7520–7533. [CrossRef] [PubMed]
6. Farthing, D.E.; Farthing, C.A.; Xi, L. Inosine and hypoxanthine as novel biomarkers for cardiac ischemia: From bench to point-of-care. *Exp. Biol. Med.* **2015**, *240*, 821–831. [CrossRef]
7. Lee, J.S.; Wang, R.X.; Alexeev, E.E.; Lanis, J.M.; Battista, K.D.; Glover, L.E.; Colgan, S.P. Hypoxanthine is a checkpoint stress metabolite in colonic epithelial energy modulation and barrier function. *J. Biol. Chem.* **2018**, *293*, 6039–6051. [CrossRef] [PubMed]
8. Casali, E.; Berni, P.; Spisni, A.; Baricchi, R.; Pertinhez, T.A. Hypoxanthine: A new paradigm to interpret the origin of transfusion toxicity. *Blood Transfus.* **2016**, *14*, 555–556.
9. Zieliński, J.; Krasińska, B.; Kusy, K. Hypoxanthine as a Predictor of Performance in Highly Trained Athletes. *Int. J. Sports Med.* **2013**, *34*, 1079–1086. [CrossRef]
10. Zieliński, J.; Kusy, K. Hypoxanthine: A Universal Metabolic Indicator of Training Status in Competitive Sports. *Exerc. Sport Sci. Rev.* **2015**, *43*, 214–221. [CrossRef]
11. Lawal, A.T.; Adeloju, S.B. Polypyrrole-Based Xanthine Oxidase Potentiometric Biosensor for Hypoxanthine. *J. Appl. Sci.* **2008**, *8*, 2599–2605. [CrossRef]
12. Hernández-Cázares, A.S.; Aristoy, M.C.; Toldrá, F. Hypoxanthine-based enzymatic sensor for determination of pork meat freshness. *Food Chem.* **2010**, *123*, 949–954. [CrossRef]
13. Escrivà, E.; García-Lozano, J.; Martínez-Lillo, J.; Nuñez, H.; Server-Carrió, J.; Soto, L.; Carrasco, R.; Cano, J. Synthesis, Crystal Structure, Magnetic Properties, and Theoretical Studies of [{Cu(mepirizole)Br}$_2$(μ-OH)(μ-pz)] (Mepirizole = 4-Methoxy-2-(5-methoxy-3-methyl-1H-pyrazol-1-yl)-6-methylpyrimidine; pz = Pyrazolate), a Novel μ-Pyrazolato−μ-Hydroxo-Dibridged Copper(II) Complex. *Inorg. Chem.* **2003**, *42*, 8328–8336. [PubMed]
14. Armentano, D.; Marino, N.; Mastropietro, T.F.; Martínez-Lillo, J.; Cano, J.; Julve, M.; Lloret, F.; De Munno, G. Self-Assembly of a Chiral Carbonate- and Cytidine-Containing Dodecanuclear Copper(II) Complex: A Multiarm-Supplied Globular Capsule. *Inorg. Chem.* **2008**, *47*, 10229–10231. [CrossRef] [PubMed]
15. Marino, N.; Armentano, D.; Mastropietro, T.F.; Julve, M.; De Munno, G.; Martínez-Lillo, J. Cubane-Type Cu^{II}_4 and $Mn^{II}_2Mn^{III}_2$ Complexes Based on Pyridoxine: A Versatile Ligand for Metal Assembling. *Inorg. Chem.* **2013**, *52*, 11934–11943. [CrossRef] [PubMed]
16. Armentano, D.; Barquero, M.A.; Rojas-Dotti, C.; Moliner, N.; De Munno, G.; Brechin, E.K.; Martínez-Lillo, J. Enhancement of Intermolecular Magnetic Exchange through Halogen···Halogen Interactions in Bisadeninium Rhenium(IV) Salts. *Cryst. Growth Des.* **2017**, *17*, 5342–5348. [CrossRef]
17. Orts-Arroyo, M.; Castro, I.; Lloret, F.; Martínez-Lillo, J. Field-induced slow relaxation of magnetisation in two one-dimensional homometallic dysprosium(III) complexes based on alpha- and beta-amino acids. *Dalton Trans.* **2020**, *49*, 9155–9163. [CrossRef] [PubMed]
18. Rojas-Dotti, C.; Martínez-Lillo, J. Thioester-functionalised and oxime-based hexametallic manganese(III) single-molecule magnets. *RSC Adv.* **2017**, *7*, 48841–48847. [CrossRef]
19. Tyagi, P.; Riso, C.; Amir, U.; Rojas-Dotti, C.; Martínez-Lillo, J. Exploring room-temperature transport of single-molecule magnet-based molecular spintronics devices using the magnetic tunnel junction as a device platform. *RSC Adv.* **2020**, *10*, 13006–13015. [CrossRef]
20. Chen, P.; Goldberg, D.E.; Kolb, B.; Lanser, M.; Benowitz, L.I. Inosine induces axonal rewiring and improves behavioral outcome after stroke. *Proc. Natl. Acad. Sci. USA* **2002**, *99*, 9031–9036. [CrossRef]
21. Kline, P.C.; Schramm, V.L. Purine Nucleoside Phosphorylase. Inosine Hydrolysis, Tight Binding of the Hypoxanthine Intermediate, and Third-the-Sites Reactivity. *Biochemistry* **1992**, *31*, 5964–5973. [CrossRef] [PubMed]
22. Jelińska, A. Kinetics of hydrolysis of inosine in aqueous solutions. *React. Kinet. Catal. Lett.* **2001**, *72*, 93–100. [CrossRef]
23. Chifotides, H.T.; Dunbar, K.R.; Matonic, J.H.; Katsaros, N. Unusual structural features of tetrakis(μ-carboxylato)dirhodium(II), an antitumor agent, bound to azathioprine, a biologically active mercaptopurine derivative. *Inorg. Chem.* **1992**, *31*, 4628–4634. [CrossRef]
24. Karran, P.; Attard, N. Thiopurines in current medical practice: Molecular mechanisms and contributions to therapy-related cancer. *Nat. Rev. Cancer* **2008**, *8*, 24–36. [CrossRef]
25. Jones, N.R.; Murray, J.; Livingston, E.I.; Murray, C.K. Rapid estimations of hypoxanthine concentrations as indices of the freshness of chill-stored fish. *J. Sci. Food Agric.* **1964**, *15*, 763–774. [CrossRef]
26. Cooper, N.; Khosravan, R.; Erdmann, C.; Fiene, J.; Lee, J.W. Quantification of uric acid, xanthine and hypoxanthine in human serum by HPLC for pharmacodynamic studies. *J. Chromatogr. B* **2006**, *837*, 1–10. [CrossRef]
27. Farthing, D.; Sica, D.; Gehr, T.; Wilson, B.; Fakhry, I.; Larus, T.; Farthing, C.; Karnes, H.T. An HPLC method for determination of inosine and hypoxanthine in human plasma from healthy volunteers and patients presenting with potential acute cardiac ischemia. *J. Chromatogr. B* **2007**, *854*, 158–164. [CrossRef]
28. Xiang, L.W.; Li, J.; Lin, J.M.; Li, H.F. Determination of gouty arthritis' biomarkers in human urine using reversed-phase high-performance liquid chromatography. *J. Pharm. Anal.* **2014**, *4*, 153–158. [CrossRef]
29. Bory, C.; Chantin, C.; Boulieu, R. Comparison of capillary electrophoretic and liquid chromatographic determination of hypoxanthine and xanthine for the diagnosis of xanthinuria. *J. Chromatogr. A* **1996**, *730*, 329–331. [CrossRef]

30. Bory, C.; Chantin, C.; Boulieu, R. Capillary Electrophoretic Analysis of Hypoxanthine and Xanthine for the Diagnosis of Xanthinuria. In *Purine and Pyrimidine Metabolism in Man IX*; Griesmacher, A., Müller, M.M., Chiba, P., Eds.; Advances in Experimental Medicine and Biology; Springer: Boston, MA, USA, 1998; Volume 431.
31. Klinenberg, J.R.; Goldfinger, S.; Bradley, K.H.; Seegmiller, J.E. An enzymatic spectrophotometric method for the determination of xanthine and hypoxanthine. *Clin. Chem.* **1967**, *10*, 834–846. [CrossRef]
32. Khajehsharifi, H.; Pourbasheer, E. Simultaneous spectrophotometric determination of xanthine, hypoxanthine and uric acid in real matrix by orthogonal signal correction-partial least squares. *J. Iran. Chem. Soc.* **2011**, *8*, 1113–1119. [CrossRef]
33. Zhang, Y.; Deng, S.; Lei, J.; Xu, Q.; Ju, H. Carbon nanospheres enhanced electrochemiluminescence of CdS quantum dots for biosensing of hypoxanthine. *Talanta* **2011**, *85*, 2154–2158. [CrossRef] [PubMed]
34. Zuo, F.; Zhang, H.; Xie, J.; Chen, S.; Yuan, R. A sensitive ratiometric electrochemiluminescence biosensor for hypoxanthine detection by in situ generation and consumption of coreactants. *Electrochim. Acta* **2018**, *271*, 173–179. [CrossRef]
35. Dou, Z.-Y.; Cui, L.-L.; He, X.Q. Electrochimical determination of uric acid, xanthine and hypoxanthine by poly(xylitol) modified glassy carbon electrode. *J. Cent. South Univ.* **2014**, *21*, 870–876. [CrossRef]
36. Mardini-Farias, P.A.; Castro, A.A. Determination of Xanthine in the Presence of Hypoxanthine by Adsorptive Stripping Voltammetry at the Mercury Film Electrode. *Anal. Chem. Insights* **2014**, *9*, 49–55. [CrossRef]
37. Juban, K.B.B.; Billones, J.B. Simultaneous Electrochemical Determination of Hypoxanthine and Xanthine by Poly(Threonine) Film-Modified Electrode. *Anal. Bioanal. Electrochem.* **2015**, *7*, 149–160.
38. *SHELXTL-2017/1, Bruker Analytical X-ray Instruments*; Bruker: Madison, WI, USA, 2017.
39. *DIAMOND 4.5.0, Crystal Impact GbR*; Crystal Impact: Bonn, Germany, 2018.
40. Armentano, D.; Martínez-Lillo, J. Hexachlororhenate(IV) salts of ruthenium(III) cations: X-ray structure and magnetic properties. *Inorg. Chim. Acta* **2012**, *380*, 118–124. [CrossRef]
41. Orts-Arroyo, M.; Castro, I.; Lloret, F.; Martínez-Lillo, J. Molecular Self-Assembly in a Family of Oxo-Bridged Dinuclear Ruthenium(IV) Systems. *Cryst. Growth Des.* **2020**, *20*, 2044–2056. [CrossRef]
42. Dubler, E.; Hänggi, G.; Schmalle, H. Synthesis and structure of dimeric metal complexes with N(3)/N(9)-chelating hypoxanthine ligands and with bridging water molecules: $[M_2(\mu\text{-hyxan})_2(SO_4)_2(\mu\text{-}H_2O)_2(H_2O)_2]$ (M = copper, cadmium, zinc; hyxan = hypoxanthine). *Inorg. Chem.* **1990**, *29*, 2518–2523. [CrossRef]
43. Hänggi, G.; Schmalle, H.; Dubler, E. Structure of $[Co_2(\mu\text{-hypoxanthine})_2(SO_4)_2(\mu\text{-}H_2O)_2(H_2O)_2]$. *Acta Cryst.* **1992**, *C48*, 1008–1012.
44. Reid, J.; Bond, T.; Wang, S.; Zhou, J.; Hu, A. Synchrotron powder diffraction, X-ray absorption and 1H nuclear magnetic resonance data for hypoxanthine. *Powder Diffr.* **2015**, *30*, 278–285. [CrossRef]
45. Mohite, S.S.; Patil-Deshmukh, A.B.; Chavan, S.S. Synthesis and characterization of Ru(III) complexes with 2-((E)-((4-((4-bromophenyl)ethynyl)phenyl)imino)methyl-4-((E)-phenyldiazenyl)phenol and their use as a precursor for RuO_2 nanoparticles. *J. Mol. Struct.* **2019**, *1176*, 386–393. [CrossRef]
46. Sur, V.P.; Mazumdar, A.; Kopel, P.; Mukherjee, S.; Vítek, P.; Michalkova, H.; Vaculovičová, M.; Moulick, A. A Novel Ruthenium Based Coordination Compound Against Pathogenic Bacteria. *Int. J. Mol. Sci.* **2020**, *21*, 2656. [CrossRef] [PubMed]
47. Shahrokhian, S.; Ghalkhani, M. Electrochemical study of Azathioprine at thin carbon nanoparticle composite film electrode. *Electrochem. Commun.* **2009**, *11*, 1425–1428. [CrossRef]
48. Rao, C.N.; Balaji, K.; Venkateswarlu, P. Determination of azathioprine and rocuronium in biological fluid samples by voltammetry. *Biomed. Pharmacol. J.* **2009**, *2*, 117–121.
49. Jalali, F.; Rasaee, G. Electrochemical, spectroscopic, and theoretical studies on theinteraction between azathioprine and DNA. *Int. J. Biol. Macromol.* **2015**, *81*, 427–434. [CrossRef]
50. Asadian, E.; Iraji Zad, A.; Shahrokhian, S. Voltammetric studies of Azathioprine on the surface of graphite electrodemodified with graphene nanosheets decorated with Ag nanoparticles. *Mater. Sci. Eng. C* **2016**, *58*, 1098–1104. [CrossRef]
51. Oliveira-Brett, A.M.; Silva, L.A.; Farace, G.; Vadgama, P.; Brett, C.M.A. Voltammetric and impedance studies of inosine-5′-monophosphate and hypoxanthine. *Bioelectrochemistry* **2003**, *59*, 49–56. [CrossRef]
52. Revin, S.B.; John, S.A. Selective determination of inosine in the presence of uric acid and hypoxanthine using modified electrode. *Anal. Biochem.* **2012**, *421*, 278–284. [CrossRef]
53. Cotton, F.A.; Pedersen, E. Magnetic and electrochemical properties of transition metal complexes with multiple metal-to-metal bonds. II. Tetrabutyratodiruthenium(n+) with n = 0 and 1. *Inorg. Chem.* **1975**, *14*, 388–391. [CrossRef]
54. Malinski, T.; Chang, D.; Feldmann, F.N.; Bear, J.L.; Kadish, K.M. Electrochemical studies of a novel ruthenium(II, III) dimer, trifluoroacetamidatoruthenium chloride ($Ru_2(HNOCCF_3)_4Cl$). *Inorg. Chem.* **1983**, *22*, 3225–3233. [CrossRef]
55. Hiraoka, Y.; Ikeue, T.; Sakiyama, H.; Guégan, F.; Luneau, D.; Gillon, B.; Hiromitsu, I.; Yoshioka, D.; Mikuriya, M.; Kataoka, Y.; et al. An unprecedented up-field shift in the ^{13}C NMR spectrum of the carboxyl carbons of the lantern-type dinuclear complex $TBA[Ru_2(O_2CCH_3)_4Cl_2]$ (TBA^+ = tetra(n-butyl)ammonium cation). *Dalton Trans.* **2015**, *44*, 13439–13443. [CrossRef] [PubMed]
56. Kataoka, Y.; Mikami, S.; Sakiyama, H.; Mitsumi, M.; Kawamoto, T.; Handa, M. A neutral paddlewheel-type diruthenium(III) complex with benzamidinato ligands: Synthesis, crystal structure, magnetism, and electrochemical and absorption properties. *Polyhedron* **2017**, *136*, 87–92. [CrossRef]